Antti H. Niemi. 2008. Approximation of shell layers using bilinear elements on anisotropically refined rectangular meshes. Computer Methods in Applied Mechanics and Engineering, volume 197, numbers 45-48, pages 3964-3975.

Comput. Methods Appl. Mech. Engrg. 197 (2008) 3964–3975

Contents lists available at ScienceDirect

Comput. Methods Appl. Mech. Engrg.

journal homepage: www.elsevier.com/locate/cma

Approximation of shell layers using bilinear elements on anisotropically refined rectangular meshes

Antti H. Niemi

Institute of Mathematics, Helsinki University of Technology, P.O. Box 1100, Espoo FI-02015 TKK, Finland

ARTICLE INFO

Article history:
Received 12 November 2007
Received in revised form 18 March 2008
Accepted 22 March 2008
Available online 3 April 2008

Keywords:
Finite elements
Shells
Locking
Shell layers

ABSTRACT

In this paper, we study numerical locking effects in the finite element approximation of shell layers. The focus is on four-node degenerated elements that are perhaps the most widely used in practical computations. Our approach is based on simplified reformulations of the original 3D elements in the context of a classical shallow shell model, where the deformation of the shell is described in terms of the three displacements of the middle surface and two dimensionless rotations related to transverse shear deformations. Within that model we compute finite element approximations of layers generated by smooth line segments such as the boundary line. Our numerical results show that approximation failure occurs when bilinear degenerated elements are used on anisotropically refined meshes and that the accuracy depends substantially on the specific geometry of the shell. By analyzing the layers as functions of the thickness of the shell, we obtain theoretical error estimates in the energy norm framework that predict error amplification for small values of the thickness. The error estimates are then verified by conducting further numerical experiments using overrefined meshes.

1. Introduction

Generally speaking, a shell structure resists external loads by combining membrane and bending action through its curvature. However, in the detailed analysis one usually has in mind two important special cases, a *bending-dominated* deformation state and a *membrane-dominated* deformation state. In the design one should always pursue the membrane state since pure bending leads to remarkable deflections of the shell in view of its small thickness. Unfortunately the identification of *inextensional* displacement fields using standard finite element procedures is very difficult because of *membrane and shear locking*. A large number of research papers has been devoted to this problem throughout the history of finite elements without final success so far as regards mathematical error analysis, at least. Even if "locking-free" methods have been constructed and analyzed in the mathematical literature, they are usually tailored for bending-dominated deformations only and tend to cause unwanted error growth in membrane-dominated cases, see e.g. [1,2]. In these cases standard procedures would work essentially as well as in any classical elliptic boundary value problem.

On the other hand, one of the oldest remedies for the above difficulties is to approximate the curved shell first by flat elements and then superimpose plate bending stiffness with membrane stiffness (see [3, Chapter 6] for a survey of this kind of methodology). Relatively simple formulations involving four-node plate elements with bilinear shape functions have turned out to be competitive for shells that can be well represented using flat elements. Anyway, most of the modern shell element libraries are based on isoparametric finite element techniques (the so called degenerated 3D approach, see [4,5]) so that four-node elements can be applied also to general shells as straight-sided but not necessary flat quadrilaterals. In fact, such elements are often considered among the best general purpose shell elements and they seem to be the workhorses of many commercial finite element codes such as ABAQUS and ADINA.

Although geometrically incompatible finite element models have been used for decades in structural analysis of shells, the mathematical theory underlying them is still in its infancy. This is not so surprising since the mathematical understanding of shell deformations is mainly based on the classical shell theory which was written for the most part before the invention of finite elements and computers. The reformulation of the numerical models in the context of 2D shell models is not very straightforward albeit an analogous approach has been applied successfully to circular arches by Kikuchi in [6] and later on to more general curved rods by Chapelle in [7]. The mathematical properties of triangular facet elements have been discussed in the works of Bernadou et al. (see [8, Part III] and the references therein), whereas the relation between classical shell models and the degenerated 3D approach has been investigated by Büchter and Ramm in [9] and by Chapelle and Bathe in [10], see also [11].

But then Malinen has provided a framework for mathematical error analysis of bilinear degenerated elements in [12,13] by formulating the original elements nearly equivalently within a classical 2D shell model. The connection reveals in particular how these

E-mail address: antti.h.niemi@tkk.fi

0045-7825/$ - see front matter © 2008 Elsevier B.V. All rights reserved.
doi:10.1016/j.cma.2008.03.021

formulations avoid membrane locking at least under favorable conditions by a clever approximation of (nearly) inextensional deformations. However, evidence of unwanted error growth is obtained when the displacement field considered is subject to fast variations as near boundaries, junctions and irregular loads where the layers are strong. Actually a similar observation was made in [14] by Andelfinger and Ramm.

In this paper we bring to light the numerical locking effects associated to the finite element approximation of shell layers using bilinear elements on anisotropically refined meshes. In addition to a good understanding of the numerical properties of the bilinear degenerated 3D FEM, we need knowledge of the asymptotic nature of shell deformations beyond the usual membrane and inextensional theories. In the classical literature on the theory of shells (see [15,16]) the layers are known as "edge effects", but their treatment there is rather limited from the modern perspective. Nevertheless, a more systematic asymptotic and numerical analysis of these phenomena has restarted fairly recently e.g. in [17–23].

Here we consider layers generated by a smooth line segment S and concentrate on the following main layer modes in shell deformations:

1. The line layer that decays in the length scale $L \sim \sqrt{Rt}$ from S, where t is the thickness of the shell and R measures the total curvature of the shell. This layer is possible in all shell geometries.
2. The line layer that decays in the length scale $L \sim \sqrt[3]{R^2 t}$ from S. This arises in hyperbolic shell geometry when S is a characteristic line of the middle surface of the shell.
3. The line layer that decays in the length scale $L \sim \sqrt[4]{R^3 t}$ from S. This layer is possible when S is the characteristic line of a parabolic middle surface.

Since the shell deviates only slightly from a plane in the decay length scales, the shallow shell model derived by Pitkäranta et al. in [17] serves as a natural starting point for our study. By treating S as a straight line within that model, we introduce an analytically solvable model problem where the shell is under a concentrated line load that varies smoothly along S. Our numerical models are based on the standard bilinear scheme for the 2D shell model but the strain expressions are modified in accordance with the geometric and physical assumptions of the original 3D elements.

It is known from the existing finite element theory on shell layers, see [17], that (anisotropic) shear locking occurs in each of these cases when the simplest conforming finite element models are used. In addition, the degenerated Cases 2 and 3 give rise to membrane locking effects which has been noted also in [22,23,21].

Concerning geometrically incompatible formulations, our computations show that approximation failure occurs in all of the above cases when anisotropically refined meshes are used, and that the case of hyperbolic degeneration (Case 2) appears to be the worst in this sense. On the other hand, geometrically compatible elements based on the shallow shell theory approach appear to be more efficient here provided that the membrane strains are modified very carefully. The conclusion is that when approximating shell layers, the replacement of the shell middle surface locally by its isoparametric bilinear approximation, or *faceting*, is not the best choice among the possible *numerical tricks* aiming at avoiding locking.

Our computational observations are supported also by theoretical error estimates (see Proposition 1 below) showing that for bilinear degenerated elements the relative error in the energy norm depends on the dimensionless thickness t/R and becomes severely amplified as $t/R \to 0$. More precisely, the optimal error bound for the lowest-order FEM is magnified by factors $(R/t)^{1/2}$, $(R/t)^{2/3}$ and $(R/t)^{1/4}$ in Cases 1, 2 and 3, respectively. Note that in the conforming, geometrically compatible finite element models the corresponding factors arising from membrane locking effects would be 1, $(R/t)^{1/3}$ and $(R/t)^{1/2}$, see [17] and Section 4 below. On the other hand, our study shows that a careful reduction of the geometrically compatible membrane strains can avoid the error amplification completely at least when the mesh is rectangular and aligned with the layer.

The plan of the paper is as follows. The model problem is posed and analyzed in Section 2. The finite element schemes are introduced in Section 3 where we also report the results of benchmark computations. Section 4 is then devoted to finite element theory and it contains the main results of this paper summarized in Proposition 1. The theoretical error estimates are verified in Section 5 by conducting further numerical experiments. Finally, in Section 6, detailed conclusions are presented.

2. Model problem

In the dimensionally reduced Reissner–Naghdi model for a shell of thickness t, the strain energy is given by the quadratic functional

$$\mathscr{A}(\mathbf{u},\mathbf{u}) = \mathscr{A}_m(\mathbf{u},\mathbf{u}) + \mathscr{A}_s(\mathbf{u},\mathbf{u}) + \mathscr{A}_b(\mathbf{u},\mathbf{u}), \tag{1}$$

where $\mathbf{u} = (u, v, w, \theta, \psi)$ is the generalized displacement field defined on the middle surface Γ and the scaled membrane, transverse shear and bending energy functionals $\mathscr{A}_m, \mathscr{A}_s, \mathscr{A}_b$ are defined by

$$\begin{aligned}
\mathscr{A}_m(\mathbf{u},\mathbf{u}) &= \int_\Gamma \Big[\nu(\beta_{11}+\beta_{22})^2 + (1-\nu)(\beta_{11}^2 + 2\beta_{12}^2 + \beta_{22}^2)\Big]\mathrm{d}\Gamma,\\
\mathscr{A}_s(\mathbf{u},\mathbf{u}) &= \frac{1-\nu}{2}\int_\Gamma (\rho_1^2 + \rho_2^2)\,\mathrm{d}\Gamma,\\
\mathscr{A}_b(\mathbf{u},\mathbf{u}) &= \frac{t^2}{12}\int_\Gamma \Big[\nu(\kappa_{11}+\kappa_{22})^2 + (1-\nu)(\kappa_{11}^2 + 2\kappa_{12}^2 + \kappa_{22}^2)\Big]\mathrm{d}\Gamma.
\end{aligned} \tag{2}$$

Here ν is the Poisson ratio of the material (isotropic and homogeneous) and β_{ij}, ρ_i, and κ_{ij} represent the membrane, transverse shear, and bending strains, respectively.

We consider as a model problem a shallow shell such that the middle surface occupies a planar domain $\Gamma = (-1,1)\times(0,2\pi)$ in the rectilinear coordinate system (x,y) and $\mathrm{d}\Gamma = \mathrm{d}x\mathrm{d}y$ in (2). The strains are associated to the displacement field $\mathbf{u}$ then as follows (see [17]):

$$\begin{aligned}
&\beta_{11} = \frac{\partial u}{\partial x} + aw, \quad \beta_{22} = \frac{\partial v}{\partial y} + bw, \quad \beta_{12} = \frac{1}{2}\left(\frac{\partial u}{\partial y} + \frac{\partial v}{\partial x}\right) + cw,\\
&\rho_1 = \theta - \frac{\partial w}{\partial x}, \quad \rho_2 = \psi - \frac{\partial w}{\partial y},\\
&\kappa_{11} = \frac{\partial \theta}{\partial x}, \quad \kappa_{22} = \frac{\partial \psi}{\partial y}, \quad \kappa_{12} = \frac{1}{2}\left(\frac{\partial \theta}{\partial y} + \frac{\partial \psi}{\partial x}\right).
\end{aligned} \tag{3}$$

Here the constants $a = b_{11}$, $b = b_{22}$, and $c = b_{12} = b_{21}$ are the components of the curvature tensor of the shell so that the shell is elliptic when $ab - c^2 > 0$, parabolic when $ab - c^2 = 0$, and hyperbolic when $ab - c^2 < 0$.

In the benchmark problem the shell is assumed to be loaded by a normal concentrated line load

$$f(x,y) = \delta(x)\cos(ky), \tag{4}$$

where the wave number k is an integer representing the load variation along the line $x = 0$. The corresponding load functional is defined by

$$\mathscr{L}(\mathbf{u}) = \int_0^{2\pi} \cos(ky) w(0,y)\,\mathrm{d}y$$

and the resulting deformation of the shell is obtained by minimizing the total energy

$$\mathscr{F}(\mathbf{u}) = \frac{1}{2}\mathscr{A}(\mathbf{u},\mathbf{u}) - \mathscr{L}(\mathbf{u}) \tag{5}$$

in the energy space $\mathscr{U}$, where we impose the kinematic constraints $u = v = w = \theta = \psi = 0$ at $x = \pm 1$ along with periodic boundary conditions at $y = 0, 2\pi$.

Concerning the geometry of the shell, the three main cases described above are obtained with the following choices:

$$\begin{aligned}&\text{Case 1}: \quad a = c = 0, \quad b \neq 0,\\ &\text{Case 2}: \quad a = b = 0, \quad c \neq 0,\\ &\text{Case 3}: \quad b = c = 0, \quad a \neq 0.\end{aligned}$$

Case 1 represents the most common occasion where the curvature along the line $x = 0$ does not vanish. Cases 2 and 3, respectively, are examples of hyperbolic and parabolic degeneration, where the curvature along the line $x = 0$ is zero, i.e., the line $x = 0$ is a characteristic line of the middle surface.

Due to the specific shape of the load (4), the displacement field that minimizes the energy functional (5) is of the form

$$\mathbf{u}(x,y) = \mathbf{U}(x) \otimes \boldsymbol{\varphi}_k(y), \tag{6}$$

where $\mathbf{U}(x) = (U(x), V(x), W(x), \Theta(x), \Psi(x))$ and

$$\boldsymbol{\varphi}_k(y) = \begin{cases} (\cos(ky), \sin(ky), \cos(ky), \cos(ky), \sin(ky)) & \text{(Cases 1, 3)},\\ (\sin(ky), \cos(ky), \cos(ky), \cos(ky), \sin(ky)) & \text{(Case 2)}. \end{cases} \tag{7}$$

Consequently, we have a one-dimensional problem only. The unknown displacement field $\mathbf{U}(x)$ is determined from the Euler equations of the reduced energy principle (1)–(2) where now $\Gamma = (-1, 1)$, $\mathrm{d}\Gamma = \mathrm{d}x$ and

$$\begin{aligned}&\beta_{11} = U'(x) + aW(x), \quad \beta_{22} = \pm kV(x) + bW(x),\\ &\beta_{12} = \frac{1}{2}(\mp kU(x) + V'(x)) + cW(x),\\ &\rho_1 = \Theta(x) - W'(x), \quad \rho_2 = \Psi(x) + kW(x),\\ &\kappa_{11} = \Theta'(x), \quad \kappa_{22} = k\Psi(x), \quad \kappa_{12} = \frac{1}{2}(-k\Theta(x) + \Psi'(x)).\end{aligned}$$

Here the upper signs correspond to the Cases 1,3 and the lower signs to the Case 2. Due to the assumed boundary conditions at $x = \pm 1$, the solution is symmetric with respect to x. The Euler equations for the interval $0 < x < 1$ are

$$\begin{aligned}0 &= -\frac{\partial T_{11}}{\partial x} \mp kT_{12},\\ 0 &= \pm kT_{22} - \frac{\partial T_{12}}{\partial x},\\ 0 &= aT_{11} + bT_{22} + 2cT_{12} + \frac{\partial N_1}{\partial x} + kN_2,\\ 0 &= N_1 - \frac{\partial M_{11}}{\partial x} - kM_{12},\\ 0 &= N_2 + kM_{22} - \frac{\partial M_{12}}{\partial x},\end{aligned} \tag{8}$$

where the scaled membrane, shear and bending stress resultants T_{ij}, N_i and M_{ij} are defined by

$$\begin{aligned}&T_{11} = \beta_{11} + \nu\beta_{22}, \quad T_{22} = \nu\beta_{11} + \beta_{22}, \quad T_{12} = (1-\nu)\beta_{12},\\ &N_1 = \frac{1}{2}(1-\nu)\rho_1, \quad N_2 = \frac{1}{2}(1-\nu)\rho_2,\\ &M_{11} = \frac{t^2}{12}(\kappa_{11} + \nu\kappa_{22}), \quad M_{22} = \frac{t^2}{12}(\nu\kappa_{11} + \kappa_{22}), \quad M_{12} = \frac{t^2}{12}(1-\nu)\kappa_{12}.\end{aligned} \tag{9}$$

The system (8) is of total order 10, so its solution may be written in terms of the eigenvalues λ_i and the eigenvectors $\mathbf{c}^i$ as

$$\mathbf{U}(x) = \sum_{i=1}^{10} a_i \mathbf{c}^i \mathrm{e}^{\lambda_i x}, \tag{10}$$

where the constants a_i are determined by imposing the boundary condition $\mathbf{U}(1) = 0$ together with the compatibility conditions

$$\begin{aligned}&\text{Cases } 1,3: \quad U(0) = 0, \quad T_{12}(0) = 0, \quad N_1(0) = \frac{1}{2}, \quad \Theta(0) = 0,\\ &\qquad\qquad M_{12}(0) = 0,\\ &\text{Case } 2: \quad T_{11}(0) = 0, \quad V(0) = 0, \quad N_1(0) = \frac{1}{2}, \quad \Theta(0) = 0,\\ &\qquad\qquad M_{12}(0) = 0.\end{aligned}$$

The eigenvalues λ_i are found as the roots of the characteristic polynomial of system (8). It is shown in [17], that the roots can be expanded as *fractional power series*, or *Puiseux series*, of t, in a sufficiently small neighborhood of 0. Depending on the geometry of the shell, the leading terms of these expansions are determined by the following equations:

$$\begin{aligned}&\text{Case 1}: \ t^2\lambda^4 + 12(1-\nu^2)b^2 = 0 \iff \lambda_{1,2,3,4} = \frac{(-12(1-\nu^2)b^2)^{1/4}}{\sqrt{t}},\\ &\text{Case 2}: \ t^2\lambda^6 - 48(1-\nu^2)c^2k^2 = 0 \iff \lambda_{1,\ldots,6} = \frac{(48(1-\nu^2)c^2k^2)^{1/6}}{\sqrt[3]{t}},\\ &\text{Case 3}: \ t^2\lambda^8 + 12(1-\nu^2)a^2k^4 = 0 \iff \lambda_{1,\ldots,8} = \frac{(-12(1-\nu^2)a^2k^4)^{1/8}}{\sqrt[4]{t}}.\end{aligned} \tag{11}$$

In Case 1 the roots are related to the so called "simple edge effect" whereas in Cases 2 and 3 the roots stand for "generalized edge effects", cf. [16]. Due to shear deformation the characteristic equation can be reduced in all cases also to the form

$$t^2\lambda^2 - 12 = 0 \iff \lambda_{9,10} = \pm\frac{\sqrt{12}}{t}$$

representing the short-range "plate layer mode". In Cases 1 and 2 the remaining roots $\lambda_{5,6,7,8}$ and $\lambda_{7,8}$, respectively, are bounded as $t \to 0$ and correspond to "long range effects", see [17].

The kinematic constraints and (11) imply then that the solution of the model problem is essentially of the *boundary layer form*

$$\mathbf{U}(x) \sim \mathrm{e}^{-\alpha x/L}\left(\mathbf{A}\cos\frac{\beta x}{L} + \mathbf{B}\sin\frac{\beta x}{L}\right), \quad \alpha, \beta = \mathscr{O}(1), \ \alpha, x > 0, \tag{12}$$

where L is the characteristic length scale of exponential decay. Assuming that $a, b, c, k \sim R^{-1}$, we will have $L \sim \sqrt[n]{R^{n-1}t}$, where $n = 2$ in Case 1, $n = 3$ in Case 2, and $n = 4$ in Case 3.

Note that when t is small, the system of equations determining the constants a_i is ill-conditioned, but it can be solved by a computer program such as Mathematica or Maple that can compute with arbitrary high precision, cf. [24].

3. Benchmark computations

In this section, the model problem is solved approximately by the finite element method without exploiting the trigonometric variation of the solution. As in [25], the computational domain is restricted to $\Gamma = (0, 1) \times (0, \pi/4)$ by imposing symmetry/antisymmetry boundary conditions along the lines $x = 0$, $y = 0$ and $y = \pi/4$. The finite element models are based on rectangular subdivisions of Γ with piecewise uniform $(M + Q) \times N$ grids, see Fig. 1. Here M denotes the number of mesh intervals in the x-direction on the zone $0 < x < 4L$ where the layer solutions have a significant amplitude. The mesh parameter Q determines the number of mesh intervals in the x-direction away from the layer zone and the parameter N in the y-direction throughout the computational domain Γ.

In the following we consider one of the simplest approaches where the five displacement components are approximated independently by bilinear elements and the strain energy functional is modified numerically in order to avoid parametric locking effects. Concerning the transverse shear strains, the wide engineering literature (see e.g. [26–29]) supports the modifications

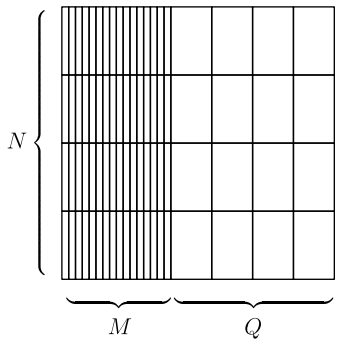

Fig. 1. An anisotropically refined rectangular mesh used in numerical computations.

$$\rho_1 \hookrightarrow \Pi_x \rho_1, \quad \rho_2 \hookrightarrow \Pi_y \rho_2, \tag{13}$$

where Π_x and Π_y are local averaging operators defined on each rectangular element $K = (x_i, x_{i+1}) \times (y_j, y_{j+1}) \subset \Gamma$ by

$$(\Pi_x f)(x,y) = \frac{1}{x_{i+1} - x_i} \int_{x_i}^{x_{i+1}} f(x',y)\,\mathrm{d}x', \tag{14}$$

$$(\Pi_y f)(x,y) = \frac{1}{y_{j+1} - y_j} \int_{y_j}^{y_{j+1}} f(x,y')\,\mathrm{d}y'. \tag{15}$$

Note that while these strain reductions can be achieved by any of the above cited methods, the different methods will lead to slightly different results on more general meshes.

On the other hand, the local replacement of the shell middle surface by its isoparametric bilinear approximation corresponds to the modification of the membrane strains as follows (see [13]):

$$\begin{aligned}
\beta_{11} &\hookrightarrow \frac{\partial u}{\partial x} + a\Pi_x w + cR_y w,\\
\beta_{22} &\hookrightarrow \frac{\partial v}{\partial y} + b\Pi_y w + cR_x w,\\
\beta_{12} &\hookrightarrow \frac{1}{2}\left(\frac{\partial u}{\partial y} + \frac{\partial v}{\partial x} + c(\Pi_x w + \Pi_y w) + aR_x w + bR_y w\right).
\end{aligned} \tag{16}$$

Here Π_x, Π_y are the averaging operators defined above whereas R_x, R_y can be expressed on the reference element $\hat{K} = (-1,1)\times(-1,1)$ as

$$(\widehat{R}_x \hat{f})(\hat{x},\hat{y}) = \frac{1}{4}(x_{i+1} - x_i)[(1+\hat{x})\partial_y F_{i+1}^j - (1-\hat{x})\partial_y F_i^j], \tag{17}$$

$$(\widehat{R}_y \hat{f})(\hat{x},\hat{y}) = \frac{1}{4}(y_{j+1} - y_j)[(1+\hat{y})\partial_x F_i^{j+1} - (1-\hat{y})\partial_x F_i^j], \tag{18}$$

where $\partial_x F_i^j$ and $\partial_y F_i^j$ are the forward difference quotients with respect to x and y,

$$\partial_x F_i^j = \frac{f(x_{i+1},y_j) - f(x_i,y_j)}{x_{i+1} - x_i} \quad \text{and} \quad \partial_y F_i^j = \frac{f(x_i,y_{j+1}) - f(x_i,y_j)}{y_{j+1} - y_j}.$$

The analysis in [13] shows also that if the displacement field is inextensional with $\beta_{11} = \beta_{22} = 0$, then the modification (16) amounts to averaging the membrane strains as

$$\beta_{11} \hookrightarrow \Pi_x \beta_{11}, \quad \beta_{22} \hookrightarrow \Pi_y \beta_{22}, \quad \beta_{12} \hookrightarrow \Pi_{xy} \beta_{12}, \tag{19}$$

where Π_{xy} is a local averaging operator defined for each K by

$$(\Pi_{xy} f)(x,y) = \frac{1}{(x_{i+1} - x_i)(y_{j+1} - y_j)} \int_{y_j}^{y_{j+1}} \int_{x_i}^{x_{i+1}} f(x',y')\,\mathrm{d}x'\mathrm{d}y'.$$

Concerning other kind of deformation states and especially boundary layers, it appears that the modification (19) is a rather favorable interpretation of the modification (16) arising from the bilinear approximation of the shell geometry, see [12]. In the following, we analyze both formulations and label the element as MITC4-F when using the modification (16) and as MITC4-S when using the modification (19), cf. [21,30].

In addition we consider a variant of these formulations, labeled as MITC4-R. This was introduced in [30] as a reformulation of MITC4-S so as to allow more general quadrilateral element shapes. In case of a rectangular mesh the membrane strain modifications of MITC4-R may be written as

$$\begin{aligned}
\beta_{11} &\hookrightarrow \frac{\partial u}{\partial x} + a\Pi_x w,\\
\beta_{22} &\hookrightarrow \frac{\partial v}{\partial y} + b\Pi_y w,\\
\beta_{12} &\hookrightarrow \frac{1}{2}\left(\frac{\partial u}{\partial y} + \frac{\partial v}{\partial x} + 2c\Pi_{xy} w + a\widetilde{R}_x w + b\widetilde{R}_y w\right),
\end{aligned} \tag{20}$$

where Π_x, Π_y, and Π_{xy} are as above and $\widetilde{R}_x$ and $\widetilde{R}_y$ are given on $\hat{K}$ by

$$(\widehat{\widetilde{R}}_x \hat{f})(\hat{x},\hat{y}) = \frac{1}{4}(x_{i+1} - x_i)(\partial_y F_{i+1}^j + \partial_y F_i^j)\hat{x}, \tag{21}$$

$$(\widehat{\widetilde{R}}_y \hat{f})(\hat{x},\hat{y}) = \frac{1}{4}(y_{j+1} - y_j)(\partial_x F_i^{j+1} + \partial_x F_i^j)\hat{y}, \tag{22}$$

in analogy with (17) and (18), see [30] for more details.

We turn now to numerical experiments by choosing $k = 2$, $\nu = 1/3$, $t = 1/1000$ and setting the non-vanishing curvature parameter to unity in each case. Figs. 2–4 show the transverse deflection profile on the zone $0 < x < 4L$ for the three benchmark cases, as computed with the different bilinear elements with

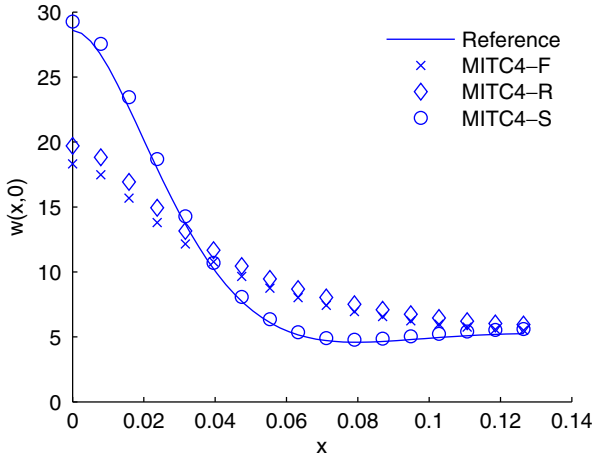

Fig. 2. Transverse deflection profile using different elements: Case 1.

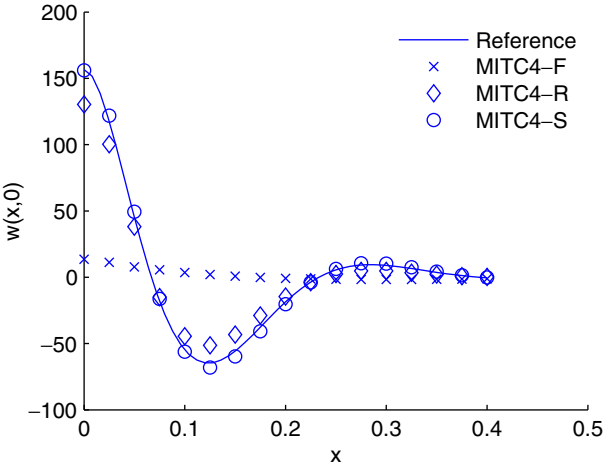

Fig. 3. Transverse deflection profile using different elements: Case 2.

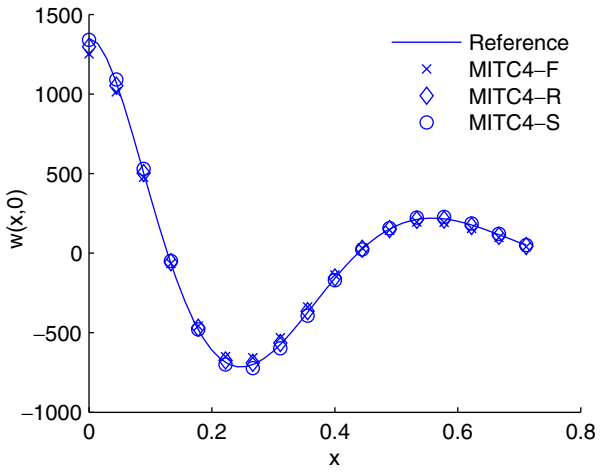

Fig. 4. Transverse deflection profile using different elements: Case 3.

$M = 16$ and $N = Q = 4$. The analytical reference solution is visualized by a solid line in all cases.

In Case 1, the performance of MITC4-F and MITC4-R is about equal but clearly inferior to MITC4-S which performs fairly well. This is to be expected since the deformation is comparable to that in Case 3 of reference [12] where the accuracy of MITC4-F (labeled there as RMITC4) was observed to deteriorate. In Case 2, the bilinear degenerated element fails almost completely. MITC4-R performs better but still gives a poor result compared with MITC4-S whose error is negligible. Finally in Case 3, all elements give good results but MITC4-S is still slightly ahead of MITC4-F and MITC4-R.

The advantage of MITC4-S over MITC4-F and MITC4-R becomes more evident in Figs. 5–7 representing the (scaled) von Mises membrane stress resultant defined by

$$T_{\mathrm{v}} = \sqrt{T_{11}^2 + T_{22}^2 - T_{11}T_{22} + 3T_{12}^2},$$

where T_{11}, T_{22} and T_{12} are defined as in (9). The stress fields of MITC4-F and MITC4-R show strong unphysical oscillations while the results of MITC4-S are good in all cases.

4. Analysis of locking effects

In this section the model problem is considered from the viewpoint of finite element theory in order to explain the numerical results of the previous section. Following the footsteps of Pitkäranta and Suri in [31–34], we use the modified variational formulation directly in our reasoning. As in [34] we start by defining the error indicator

$$e = \frac{|||\mathbf{u} - \mathbf{u}_h|||_h}{|||\mathbf{u}|||}, \tag{23}$$

where $|||\cdot|||$ and $|||\cdot|||_h$ are the energy norm (square root of the strain energy) and its numerical counterpart after the strain modifications (different for each element). The error indicator is obviously scaling invariant and dimensionless.

Various other error measures for the evaluation of shell finite elements are discussed in the book of Chapelle and Bathe [35] where the so called "s-norm" is recommended in particular as an assessment tool. The "s-norm" measures the error by comparing the approximate strain fields with the *exact* reference strains by means of the strain energy whereas the indicator (23) uses the *modified* reference strains in the comparison. The advantage of (23) is that the total error may be split in two parts, called the *approximation error* and the *consistency error*, and these may be analyzed separately. The approximation error e_{a} is simply the error of the best approximation of $\mathbf{u}$ in terms of the modified energy norm, i.e.,

$$e_{\mathrm{a}} = \min_{\mathbf{v}\in\mathscr{U}_h} \frac{|||\mathbf{u} - \mathbf{v}|||_h}{|||\mathbf{u}|||}. \tag{24}$$

The consistency error, or *equilibrium error*, e_{c} arising from the modification of the variational principle is then given by

$$e_{\mathrm{c}} = \max_{\mathbf{v}\in\mathscr{U}_h} \frac{\mathscr{A}(\mathbf{u},\mathbf{v}) - \mathscr{A}_h(\mathbf{u},\mathbf{v})}{|||\mathbf{u}||| \, |||\mathbf{v}|||_h}, \tag{25}$$

where $\mathscr{A}_h(\cdot,\cdot)$ is the modified strain energy functional. The above splitting of the error is orthogonal in the sense that $e^2 = e_{\mathrm{a}}^2 + e_{\mathrm{c}}^2$, see [34].

Tables 1–3 show the error decomposition for the model problem using the different elements and the same problem setup as in the previous section. In Case 1, the bad results of MITC4-F and MITC4-R compared to MITC4-S are reflected in the value of the consistency error which is about seventy times larger for MITC4-F and MITC4-R than for MITC4-S. In Case 2, the same comparison gives factor ten for MITC4-R and nearly three hundred for MITC4-F. This is in line with the results of Figs. 3 and 6. Also the approximation error values in Case 2 are larger for MITC4-F and MITC4-R than for MITC4-S. Finally, the error values in Case 3 indicate mild amplification of both error components for MITC4-F and MITC4-R as might be expected from the results of Section 3.

To obtain a theoretical error estimate, one needs to know how $|||\mathbf{u}|||$ in the denominator of Eqs. (23)–(25) scales with respect to the thickness parameter t/R. Here we may assume that $\mathbf{u}$ is of the form (6), (12) and resolve the parametric dependence of $|||\mathbf{u}|||$ by applying the theory of [17]. Indeed, by a proper scaling of the variables and displacement amplitudes, $\mathbf{u}$ can be viewed as a smooth, non-parametric function varying in the unit range so that after normalization of the energy density one has $|||\mathbf{u}||| \sim 1$. The parametric dependence of the problem appears then merely in the scaled expressions of the strain energy functional (1) and its numerical counterpart.

In the analysis, a shorthand notation involving inner products and norms of square integrable scalar functions is used. These are defined on the (scaled) domain Γ as usual, i.e.,

$$(f,g) = \int_\Gamma fg \,\mathrm{d}x\,\mathrm{d}y, \quad \|f\| = (f,f)^{1/2}.$$

Furthermore, C denotes a generic constant which is positive, finite and independent of the dimensionless thickness t/R.

4.1. Transverse shear and bending effects

To find the scaled expressions of the bending and transverse shear energies, we rescale the coordinates x, y, the transverse displacement w, and the rotations θ, ψ as (see [17])

$$x \hookrightarrow Lx, \quad y \hookrightarrow Ry, \quad w \hookrightarrow Rw, \quad \theta \hookrightarrow L^{-1}R\theta, \quad \psi \hookrightarrow \psi. \tag{26}$$

The resulting bending energy functional takes the form

$$12\mathscr{A}_b(\mathbf{u},\mathbf{u}) = \nu\left\|\frac{\partial\theta}{\partial x} + \frac{L^2}{R^2}\frac{\partial\psi}{\partial y}\right\|^2 + (1-\nu)\left\|\frac{\partial\theta}{\partial x}\right\|^2 + \frac{1}{2}(1-\nu)\frac{L^2}{R^2}\left\|\frac{\partial\theta}{\partial y} + \frac{\partial\psi}{\partial x}\right\|^2 + (1-\nu)\frac{L^4}{R^4}\left\|\frac{\partial\psi}{\partial y}\right\|^2, \tag{27}$$

where the coefficient of the dominant term κ_{11}^2 has been normalized to unity by scaling the strain energy by factor $t^{-2}L^4R^{-2}$.

The scaled expression of the transverse shear energy functional is then written as

$$\mathscr{A}_s(\mathbf{u},\mathbf{u}) = \frac{1-\nu}{2}\frac{L^2}{t^2}\left(\left\|\theta - \frac{\partial w}{\partial x}\right\|^2 + \frac{L^2}{R^2}\left\|\psi - \frac{\partial w}{\partial y}\right\|^2\right) \tag{28}$$

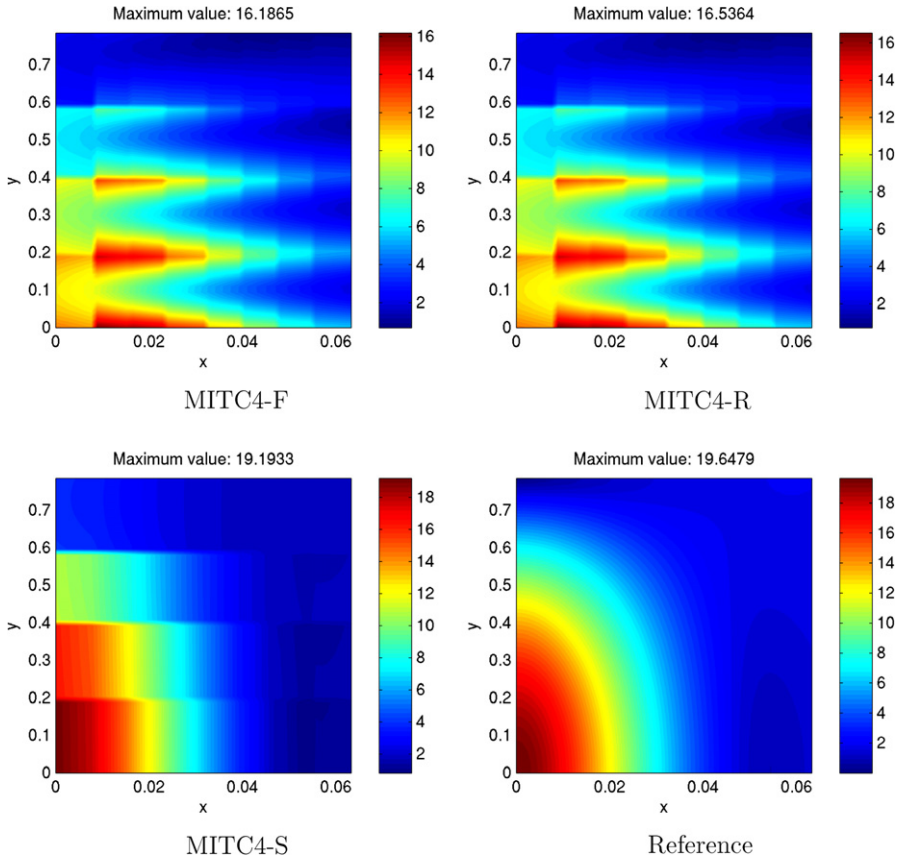

Fig. 5. Von Mises membrane stress resultant T_v using different elements: Case 1.

and its numerically modified counterpart is given by

$$\mathscr{A}_{h,s}(\mathbf{u},\mathbf{u}) = \frac{1-\nu}{2}\frac{L^2}{t^2}\left(\left\|\Pi_x\left(\theta-\frac{\partial w}{\partial x}\right)\right\|^2 + \frac{L^2}{R^2}\left\|\Pi_y\left(\psi-\frac{\partial w}{\partial y}\right)\right\|^2\right). \tag{29}$$

Obviously the operators Π_x, Π_y are not affected by the scaling of the coordinates.

We observe from (27) and (28) that when $t/L \to 0$ the energy formulation enforces the classical shear constraints

$$\theta - \frac{\partial w}{\partial x} = 0 \quad \text{(Cases 1, 2, 3)}, \tag{30}$$

$$\psi - \frac{\partial w}{\partial y} = 0 \quad \text{(Cases 2, 3)}. \tag{31}$$

It is well known that approximation failure, or locking, occurs if these are imposed as such in the numerical model. Anyway, in our case the shear constraints are reduced as

$$\Pi_x\left(\theta - \frac{\partial w}{\partial x}\right) = 0 \quad \text{(Cases 1, 2, 3)}, \tag{32}$$

$$\Pi_y\left(\psi - \frac{\partial w}{\partial y}\right) = 0 \quad \text{(Cases 2, 3)} \tag{33}$$

in order to maintain the approximation properties of the bilinear finite element space.

To bound the consistency error arising from this modification, the generalized transverse shear load functional $\mathscr{Q}(\mathbf{v}) \doteq (\mathscr{A}_s - \mathscr{A}_{h,s})(\mathbf{u},\mathbf{v})$ is written in terms of the (scaled) shear stress $\mathbf{q} = L^2/t^2(\boldsymbol{\theta} - \nabla w)$ as

$$\mathscr{Q}(\mathbf{v}) = (q_1, \phi_1 - \Pi_x\phi_1) + \frac{L^2}{R^2}(q_2, \phi_2 - \Pi_y\phi_2), \quad \mathbf{v} \in \mathscr{U}_h, \tag{34}$$

where $\mathbf{v} = (\tilde{u}, \tilde{v}, \tilde{w}, \boldsymbol{\phi}) \in \mathscr{U}_h$. The expansion follows from (28) and (29) using the identities $(\Pi_x f, \Pi_x g) = (\Pi_x f, g)$ and $(\Pi_y f, \Pi_y g) = (\Pi_y f, g)$, valid because Π_x, Π_y are averaging operators.

Both terms in (34) can be estimated using the Cauchy–Schwarz inequality and the approximation properties of Π_x, Π_y (see [34]) as

$$(q_1, \phi_1 - \Pi_x\phi_1) \leqslant \|q_1\|\|\phi_1 - \Pi_x\phi_1\| \leqslant Ch_x\|q_1\|\left\|\frac{\partial\phi_1}{\partial x}\right\| \tag{35}$$

and

$$\frac{L^2}{R^2}(q_2, \phi_2 - \Pi_y\phi_2) \leqslant Ch_y\|q_2\|\frac{L^2}{R^2}\left\|\frac{\partial\phi_2}{\partial y}\right\|, \tag{36}$$

where h_x and h_y are the dimensionless mesh parameters, i.e., the scaled mesh spacings in both coordinate directions, respectively. Assuming that $\mathbf{q}$ is smooth the final conclusion from (27), (35) and (36) is then that

$$|\mathscr{Q}(\mathbf{v})| \leqslant Ch|||\mathbf{v}|||_h \quad \forall \mathbf{v} \in \mathscr{U}_h, \tag{37}$$

where $h = \max\{h_x, h_y\}$. In other words, the equilibrium error due to the shear modification is of the uniformly optimal order $\mathscr{O}(h)$. This result indicates that the approximation failures observed in Section 3 and Tables 1–3 must arise from curvature effects. These turn out to be very case-specific and are analyzed next.

4.2. Membrane effects in Case 1

In Case 1 the consistent scaling of the tangential displacements is

$$u \hookrightarrow Lu, \quad v \hookrightarrow L^2R^{-1}v$$

and since $t^{-2}L^4R^{-2} = 1$, the corresponding membrane energy functional is given by

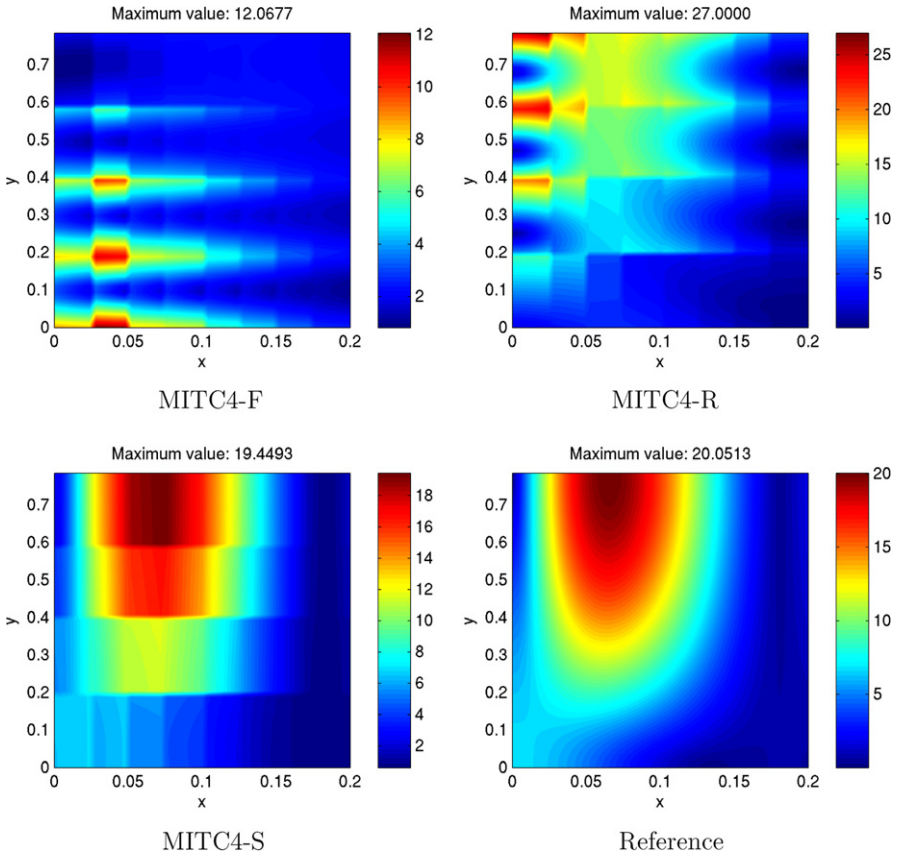

Fig. 6. Von Mises membrane stress resultant T_v using different elements: Case 2.

$$\mathscr{A}_m(\mathbf{u},\mathbf{u}) = \nu\left\|\frac{\partial u}{\partial x}+\frac{t}{R}\frac{\partial v}{\partial y}+b_0 w\right\|^2 + (1-\nu)\left\|\frac{\partial u}{\partial x}\right\|^2 + (1-\nu)\left\|\frac{t}{R}\frac{\partial v}{\partial y}+b_0 w\right\|^2 + \frac{1}{2}(1-\nu)\left\|\left(\frac{t}{R}\right)^{1/2}\left(\frac{\partial u}{\partial y}+\frac{\partial v}{\partial x}\right)\right\|^2,$$

where $b_0 = bR$ is the dimensionless curvature of the shell.

Concerning the membrane strains (16) corresponding to the bilinear geometry approximation, we note that while the averaging operators Π_x, Π_y are invariant under scaling of the coordinates x, y, the additional terms involving R_x, R_y are very sensitive to the ratio of anisotropy L/R. As a result the scaled membrane energy functional of MITC4-F involves a parametrically amplified unphysical term arising from $\beta_{12,h}$ in Case 1. The functional may be written as

$$\mathscr{A}^F_{h,m}(\mathbf{u},\mathbf{u}) = \nu\left\|\frac{\partial u}{\partial x}+\frac{t}{R}\frac{\partial v}{\partial y}+b_0\Pi_y w\right\|^2 + (1-\nu)\left\|\frac{\partial u}{\partial x}\right\|^2 + (1-\nu)\left\|\frac{t}{R}\frac{\partial v}{\partial y}+b_0\Pi_y w\right\|^2 + \frac{1}{2}(1-\nu)\left\|\left(\frac{t}{R}\right)^{1/2}\left(\frac{\partial u}{\partial y}+\frac{\partial v}{\partial x}\right)+b_0\left(\frac{R}{t}\right)^{1/2}R_y(w)\right\|^2.$$

To estimate the consistency error arising from the geometry approximation we reason that the generalized membrane load $\mathscr{T}^F(\mathbf{v}) \doteq (\mathscr{A}_m - \mathscr{A}^F_{h,m})(\mathbf{u},\mathbf{v})$ scales for $\mathbf{v} = (0,0,\tilde{w},0,0)$ like

$$|\mathscr{T}^F(\mathbf{v})| \sim \frac{R}{t}(R_y w, R_y\tilde{w}).$$

If $\tilde{w}$ is the standard interpolant of w, then $R_y w = R_y\tilde{w} = \mathscr{O}(h_y)$ since w is smooth. Summation over elements yields $\|R_y\tilde{w}\| = \mathscr{O}(h_y)$ so that we have

$$|\mathscr{T}^F(\mathbf{v})| \sim \frac{R}{t}\|R_y\tilde{w}\|^2 \sim \left(\frac{R}{t}\right)^{1/2} h_y |||\mathbf{v}|||_h. \tag{38}$$

In fact, the above reasoning holds for MITC4-R as well with $\tilde{R}_y$ replacing R_y. We conclude, combining (37) and (38), that the consistency error of MITC4-F and MITC4-R can be estimated in Case 1 as

$$e_c \sim h_x + \left(\frac{R}{t}\right)^{1/2} h_y. \tag{39}$$

For MITC4-S the scaled membrane energy is given by

$$\mathscr{A}^S_{h,m}(\mathbf{u},\mathbf{u}) = \nu\left\|\frac{\partial u}{\partial x}+\frac{t}{R}\frac{\partial v}{\partial y}+b_0\Pi_y w\right\|^2 + (1-\nu)\left\|\frac{\partial u}{\partial x}\right\|^2 + (1-\nu)\left\|\frac{t}{R}\frac{\partial v}{\partial y}+b_0\Pi_y w\right\|^2 + \frac{1}{2}(1-\nu)\left\|\left(\frac{t}{R}\right)^{1/2}\Pi_{xy}\left(\frac{\partial u}{\partial y}+\frac{\partial v}{\partial x}\right)\right\|^2.$$

Upon neglecting small terms of relative order $\mathscr{O}(t/R)$ we may expand the generalized membrane load functional $\mathscr{T}^S(\mathbf{v}) \doteq (\mathscr{A}_m - \mathscr{A}^S_{h,m})(\mathbf{u},\mathbf{v})$ for any $\mathbf{v} = (\tilde{u},\tilde{v},\tilde{w},0,0) \in \mathscr{U}_h$ as

$$\mathscr{T}^S(\mathbf{v}) = (b_0 w - \Pi_y(b_0 w), b_0\tilde{w}) + \nu\left(\frac{\partial u}{\partial x} - \Pi_y\frac{\partial u}{\partial x}, b_0\tilde{w}\right), \quad \mathbf{v} \in \mathscr{U}_h.$$

One may then conclude that (cf. [36])

$$|\mathscr{T}^S(\mathbf{v})| \leqslant Ch|||\mathbf{v}|||_h, \quad \mathbf{v} \in \mathscr{U}_h$$

when h_y is sufficiently small; hence the consistency error of MITC4-S is of optimal order uniformly with respect to the shell thickness t. Apparently also the approximation error converges with the optimal rate as the accuracy of standard interpolation is maintained under the weakened constraint (32), cf. [34].

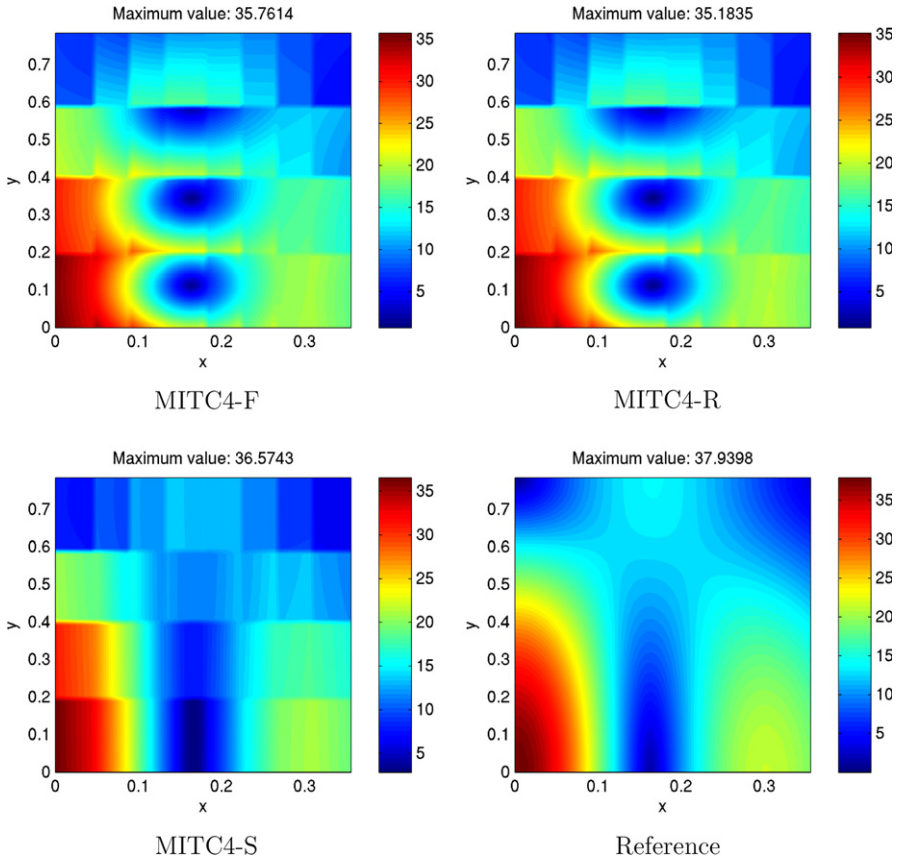

Fig. 7. Von Mises membrane stress resultant T_v using different elements: Case 3.

Table 1
Approximation and consistency errors using different elements: Case 1

	MITC4-F	MITC4-R	MITC4-S
e_a	0.105	0.102	0.102
e_c	0.718	0.653	0.012

Table 2
Approximation and consistency errors using different elements: Case 2

	MITC4-F	MITC4-R	MITC4-S
e_a	0.760	0.726	0.216
e_c	4.764	0.198	0.017

Table 3
Approximation and consistency errors using different elements: Case 3

	MITC4-F	MITC4-R	MITC4-S
e_a	0.308	0.309	0.196
e_c	0.052	0.033	0.011

4.3. Membrane effects in Case 2

In case of hyperbolic degeneration the amplitudes of the tangential displacements are rescaled as

$$u \hookrightarrow L^2R^{-1}u, \quad v \hookrightarrow Lv$$

and $t^{-2}L^4R^{-2} = (R/t)^{2/3}$ so that

$$\mathscr{A}_m(\mathbf{u},\mathbf{u}) = \nu\left\|\frac{\partial u}{\partial x}+\frac{\partial v}{\partial y}\right\|^2 + (1-\nu)\left\|\frac{\partial u}{\partial x}\right\|^2 + (1-\nu)\left\|\frac{\partial v}{\partial y}\right\|^2 + \frac{1}{2}(1-\nu)\left\|\left(\frac{t}{R}\right)^{1/3}\frac{\partial u}{\partial y}+\left(\frac{R}{t}\right)^{1/3}\left[\frac{\partial v}{\partial x}+2c_0w\right]\right\|^2,$$

where $c_0 = cR$. We note that in this case the shear constraints (30) and (31) are accompanied with the membrane constraint

$$\frac{\partial v}{\partial x}+2c_0w = 0 \tag{40}$$

at the limit $t/R = 0$. It is again obvious that the problem of locking occurs unless (40) is weakened properly in the finite element model.

Using the geometrically incompatible membrane strains (16) the scaled membrane energy takes the form

$$\mathscr{A}^F_{h,m}(\mathbf{u},\mathbf{u}) = \nu\left\|\frac{\partial u}{\partial x}+\frac{\partial v}{\partial y}+c_0\left(\frac{R}{t}\right)^{2/3}R_yw+c_0R_xw\right\|^2 + (1-\nu)\left\|\frac{\partial u}{\partial x}+c_0\left(\frac{R}{t}\right)^{2/3}R_yw\right\|^2 + (1-\nu)\left\|\frac{\partial v}{\partial y}+c_0R_xw\right\|^2 + \frac{1}{2}(1-\nu)\left\|\left(\frac{t}{R}\right)^{1/3}\frac{\partial u}{\partial y}+\left(\frac{R}{t}\right)^{1/3}\left[\frac{\partial v}{\partial x}+c_0(\Pi_xw+\Pi_yw)\right]\right\|^2.$$

We observe that the constraint (40) is replaced here by the modified constraint

$$\frac{\partial v}{\partial x}+c_0(\Pi_xw+\Pi_yw) = 0 \tag{41}$$

which implies that $\Pi_y w$ must be a constant also with respect to x when v, w are piecewise bilinear functions – still an unrealistic

requirement. Thus the approximation error of MITC4-F in Case 2 is expected to behave at best like

$$e_a \sim \left(\frac{R}{t}\right)^{1/3} h_x + h_y \tag{42}$$

so that the scheme is subject to membrane locking.

However, since the error amplification factor in (42) is smaller than the one in (39), the total failure of MITC4-F in Case 2 cannot be explained merely by estimate (42). Indeed, we conclude that the dominant error term is again the consistency error, this time due to the parametrically amplified term $R_y w$ appearing in $\beta_{11,h}$. By a similar reasoning as in Case 1 we estimate the consistency error of MITC4-F as

$$e_c \sim h_x + \left(\frac{R}{t}\right)^{2/3} h_y. \tag{43}$$

Concerning MITC4-R, there arises no additional terms in the energy expression in this case since $a = b = 0$, but the membrane constraint (40) is now replaced by

$$\frac{\partial v}{\partial x} + 2c_0 \Pi_{xy} w = 0.$$

This in turn forces $\partial^2 v/\partial x \partial y$ to be zero in the finite element space so that the error of MITC4-R in Case 2 is amplified like

$$e \sim \left(\frac{R}{t}\right)^{1/3} h.$$

For MITC4-S the membrane constraint (40) takes the weak form

$$\Pi_{xy}\left(\frac{\partial v}{\partial x} + 2c_0 w\right) = 0$$

which allows an error bound of the uniformly optimal order $\mathcal{O}(h)$, cf. [37]. In fact, Π_{xy} could be replaced by Π_x here.

4.4. Membrane effects in Case 3

Consider finally the case of parabolic degeneration. Upon scaling of the tangential displacements as

$$u \hookrightarrow Lu, \quad v \hookrightarrow L^2 R^{-1} v,$$

and noting that $t^{-2}L^4R^{-2} = R/t$, the resulting membrane energy takes the form

$$\begin{aligned}\mathcal{A}_m(\mathbf{u},\mathbf{u}) = {} & \nu \left\| \left(\frac{R}{t}\right)^{1/2} \left(\frac{\partial u}{\partial x} + a_0 w\right) + \frac{\partial v}{\partial y} \right\|^2 \\ & + (1-\nu) \left\| \left(\frac{R}{t}\right)^{1/2} \left(\frac{\partial u}{\partial x} + a_0 w\right) \right\|^2 + (1-\nu) \left\| \frac{\partial v}{\partial y} \right\|^2 \\ & + \frac{1}{2}(1-\nu) \left\| \left(\frac{R}{t}\right)^{1/4} \left(\frac{\partial u}{\partial y} + \frac{\partial v}{\partial x}\right) \right\|^2.\end{aligned}$$

This expression gives rise to two membrane constraints

$$\frac{\partial u}{\partial x} + a_0 w = 0, \tag{44}$$

$$\frac{\partial u}{\partial y} + \frac{\partial v}{\partial x} = 0, \tag{45}$$

when $t/R \to 0$. The stronger constraint (44) is weakened by all formulations cleverly as

$$\Pi_x\left(\frac{\partial u}{\partial x} + a_0 w\right) = 0, \tag{46}$$

whereas the treatment of the latter constraint is slightly different for each element. The modification of (45) involved in MITC4-F appears to be given by

$$\frac{\partial u}{\partial y} + \frac{\partial v}{\partial x} + a_0 R_x w = 0, \tag{47}$$

but, as a direct calculation using the definitions of R_x and Π_x shows, Eq. (46) can be written for piecewise bilinear u, w equivalently as

$$a_0 R_x w = \Pi_{xy} \frac{\partial u}{\partial y} - \frac{\partial u}{\partial y} + \mathcal{O}(h_x^2) \tag{48}$$

so that (47) takes effectively the form

$$\Pi_{xy} \frac{\partial u}{\partial y} + \frac{\partial v}{\partial x} = 0.$$

Table 4
Mesh overrefinement in accordance with Proposition 1

	Case 1	Case 2	Case 3
MITC4-F	$N = 4 \hookrightarrow 32$	$M = 16 \hookrightarrow 64$, $N = 4 \hookrightarrow 128$	$M = 16 \hookrightarrow 32$, $N = 4 \hookrightarrow 8$
MITC4-R	$N = 4 \hookrightarrow 32$	$M = 16 \hookrightarrow 64$, $N = 4 \hookrightarrow 16$	$M = 16 \hookrightarrow 32$, $N = 4 \hookrightarrow 8$
MITC4-S	$M = 16 \hookrightarrow 32$, $N = 4 \hookrightarrow 8$	$M = 16 \hookrightarrow 32$, $N = 4 \hookrightarrow 8$	$M = 16 \hookrightarrow 32$, $N = 4 \hookrightarrow 8$

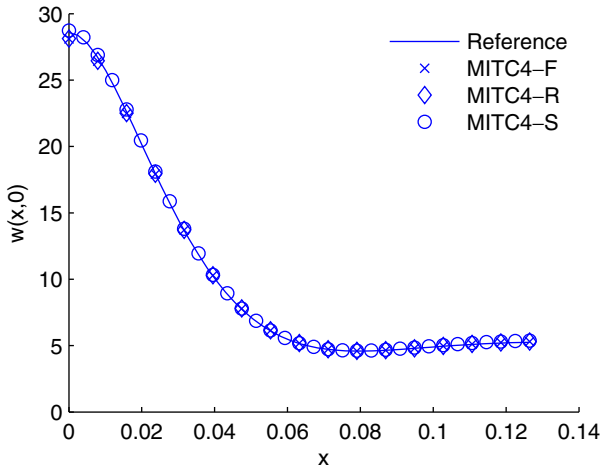

Fig. 8. Transverse deflection profile using different elements and overrefined meshes: Case 1.

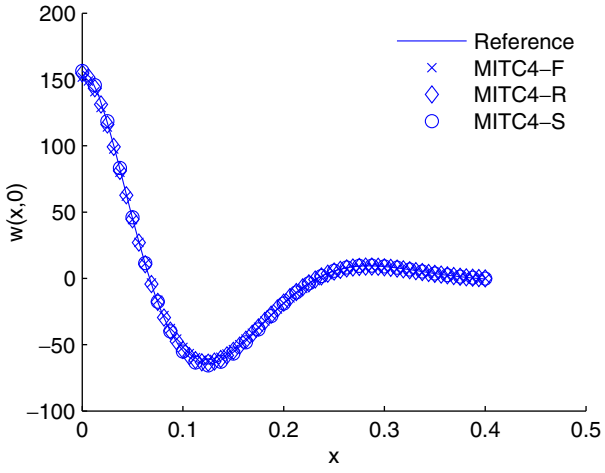

Fig. 9. Transverse deflection profile using different elements and overrefined meshes: Case 2.

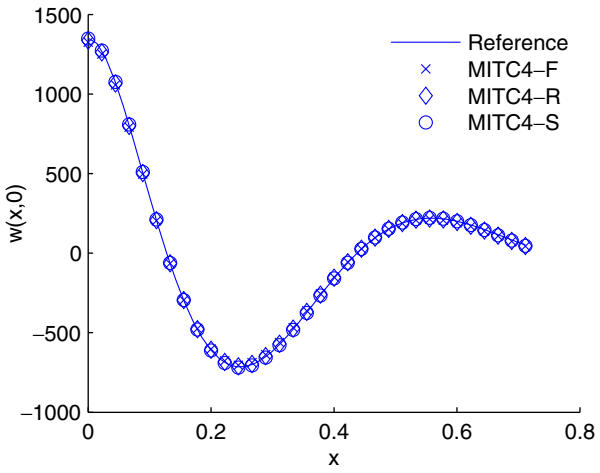

Fig. 10. Transverse deflection profile using different elements and overrefined meshes: Case 3.

In the bilinear finite element space this does not restrict u too much but enforces $\partial^2 v/\partial x\partial y$ to be zero and hence the error is expected to be amplified as

$$e \sim \left(\frac{R}{t}\right)^{1/4} h. \tag{49}$$

Note that without the additional term $a_0 R_x w$ in (47) also $\partial^2 u/\partial x\partial y$ would be restricted to zero and a more severe error amplification factor would then emerge from the constraint (46). We conclude that here (as in the case of an inextensional deformation, see [13]) the purely numerical artifact $a_0 R_x w$ is able to circumvent membrane locking to some extent.

Error estimate (49) is valid for MITC4-R as well since the above analysis goes through with $\widetilde{R}_x$ replacing R_x. In fact, Eq. (48) holds exactly without the seemingly small residual term of order $\mathcal{O}(h_x^2)$. It is possible that this detail explains the slightly better result of MITC4-R compared to MITC4-F in Fig. 4.

In MITC4-S, the latter constraint (45) is modified consistently as

$$\Pi_{xy}\left(\frac{\partial u}{\partial y}+\frac{\partial v}{\partial x}\right)=0 \tag{50}$$

and locking is expected to be completely avoided as in the previous cases.

The above development of the theory is summarized in

Proposition 1 (Error estimates). *Assume that* $\mathbf{u} \in \mathcal{U}$ *is a displacement field of the form (6), (12) and let* $\mathbf{u}_h \in \mathcal{U}_h$ *be the finite element approximation of* $\mathbf{u}$ *on a uniform rectangular mesh with scaled mesh spacing* h_x *in the x-direction and* h_y *in the y-direction, respectively. Then the total error (23) satisfies*

$$e \sim K_x h_x + K_y h_y,$$

where the factors K_x, K_y *are given for MITC4-F and MITC4-R by*

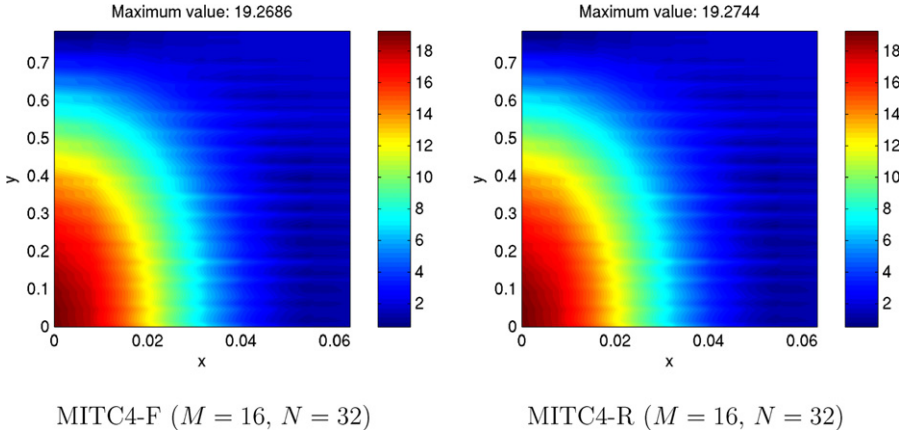

MITC4-F $(M = 16,\ N = 32)$ MITC4-R $(M = 16,\ N = 32)$

Fig. 11. Von Mises membrane stress resultant T_v using different elements and overrefined meshes: Case 1.

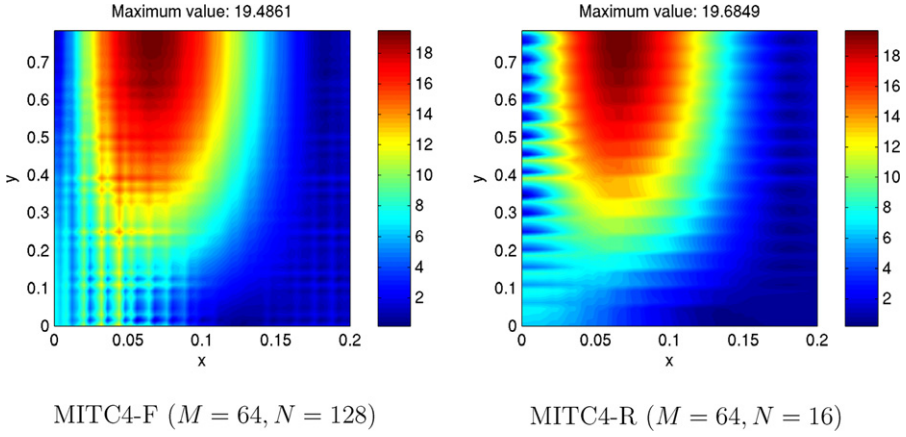

MITC4-F $(M = 64, N = 128)$ MITC4-R $(M = 64, N = 16)$

Fig. 12. Von Mises membrane stress resultant T_v using different elements and overrefined meshes: Case 2.

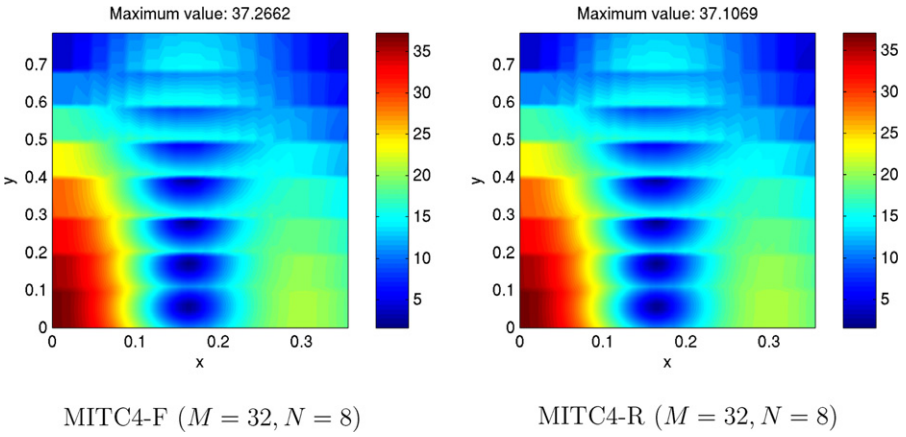

Fig. 13. Von Mises membrane stress resultant T_v using different elements and overrefined meshes: Case 3.

$$K_x \sim 1, \quad K_y \sim \left(\frac{R}{t}\right)^{1/2} \quad (\textit{Case } 1),$$

$$K_x \sim \left(\frac{R}{t}\right)^{1/3}, \quad K_y \sim \left(\frac{R}{t}\right)^{2/3} \quad (\textit{Case } 2),$$

$$K_x \sim K_y \sim \left(\frac{R}{t}\right)^{1/4} \quad (\textit{Case } 3),$$

with the exception of Case 2, where K_y is given for MITC4-R by

$$K_y \sim \left(\frac{R}{t}\right)^{1/3}.$$

Finally, if MITC4-S is used, then $K_x \sim K_y \sim 1$ in all cases.

5. Benchmark computations revisited

In this section we repeat the numerical experiments of Section 3 with overrefined finite element meshes. The overrefinement is chosen for MITC4-F and MITC4-R in each case so as to cancel the parametric error amplification predicted by Proposition 1. The mesh parameters which were used in the computations are reported in Table 4.

Table 5
Approximation and consistency errors using overrefined meshes: Case 1

	MITC4-F	MITC4-R
e_a	0.103	0.100
e_c	0.013	0.016

Table 6
Approximation and consistency errors using overrefined meshes: Case 2

	MITC4-F	MITC4-R
e_a	0.181	0.185
e_c	0.020	0.019

Table 7
Approximation and consistency errors using overrefined meshes: Case 3

	MITC4-F	MITC4-R
e_a	0.156	0.156
e_c	0.014	0.009

Figs. 8–10 show the transverse deflection on the zone $0 < x < 4L$ using the different elements. Obviously displacements are now predicted with a decent accuracy by all elements in all cases. Also the quality of the stress resultants is improved considerably although some oscillations are still present in Figs. 11–13.

The theoretical error decomposition for MITC4-F and MITC4-R is shown in Tables 5–7. Since the values are comparable to those of MITC4-S in Tables 1–3, we conclude that Proposition 1 explains the error behavior of each element quite realistically.

Note that in order to achieve feasible results with bilinear degenerated elements, the discretization must involve elements of well-balanced dimensions in the layer area. Such meshes are obviously very uneconomical when t/R is small.

6. Conclusions

We have analyzed the effect of boundary layers on the simplest quadrilateral shell elements with four nodes. Few closely related formulations have been studied in the context of classical 2D shell models. While each of these formulations incorporates mixed interpolation of transverse shear strains to overcome shear locking, the elements differ in their membrane or in-plane bending behavior.

Our study of MITC4-F shows that isoparametric bilinear elements, where the membrane strains are computed using the degenerated solid approach, are too stiff near boundaries, junctions, or load irregularities. As a result the displacement field may converge very slowly and the stress values are, in general, unreliable in regions where the layers are strong. Our mathematical analysis reveals that numerical locking occurs here because

- the consistency error arising from the use of geometrically incompatible membrane strains may become parametrically amplified when approximating layers (Cases 1 and 2),
- bilinear degenerated elements lose some of their accuracy under the (anisotropic) membrane constraints that arise when approximating layer modes decaying from a characteristic line of a hyperbolic or a parabolic shell middle surface (Cases 2 and 3).

On the other hand, the MITC4-S element, where the membrane strains are computed and modified locally in accordance with the shallow shell theory, is able to maintain the optimal accuracy of lowest-order FEM on aligned rectangular meshes. Further studies are necessary to find out to what extent the same level of accuracy

can be achieved within the degenerated solid approach e.g. by the classical method of incompatible displacement modes and its generalizations, cf. [14]. In view of the present study, the approximation of the characteristic layers in hyperbolic shells seems to be rather challenging.

References

[1] D.N. Arnold, F. Brezzi, Locking free finite elements for shells, Math. Comput. 66 (1997) 1–14.
[2] D. Chapelle, R. Stenberg, Stabilized finite element formulations for shells in a bending dominated state, SIAM J. Numer. Anal. 36 (1998) 32–73.
[3] O. Zienkiewicz, R. Taylor, The finite element method, Solid Mechanics, fifth ed., vol. 2, Butterworth-Heinemann, Oxford, 2000.
[4] S. Ahmad, B.M. Irons, O.C. Zienkiewicz, Analysis of thick and thin shell structures by curved finite elements, Int. J. Numer. Methods Engrg. 2 (1970) 419–451.
[5] K.-J. Bathe, Finite Element Procedures, Prentice Hall, Englewood Cliffs, 1996.
[6] F. Kikuchi, On the validity of the finite element analysis of circular arches represented by an assemblage of beam elements, Comput. Methods Appl. Mech. Engrg. 5 (1975) 253–276.
[7] D. Chapelle, A locking-free approximation of curved rods by straight beam elements, Numer. Math. 77 (1997) 299–322.
[8] M. Bernadou, Finite Element Methods for Thin Shell Problems, Wiley, New York, 1996.
[9] N. Büchter, E. Ramm, Shell theory versus degeneration-a comparison in large rotation finite element analysis, Int. J. Numer. Methods Engrg. 34 (1992) 39–59.
[10] D. Chapelle, K.-J. Bathe, The mathematical shell model underlying general shell elements, Int. J. Numer. Methods Engrg. 48 (2000) 289–313.
[11] J.C. Simo, D.D. Fox, M.S. Rifai, On a stress resultant geometrically exact shell model. II. The linear theory; computational aspects, Comput. Methods Appl. Mech. Engrg. 73 (1989) 53–92.
[12] M. Malinen, On the classical shell model underlying bilinear degenerated shell finite elements, Int. J. Numer. Methods Engrg. 52 (2001) 389–416.
[13] M. Malinen, On the classical shell model underlying bilinear degenerated shell finite elements: general shell geometry, Int. J. Numer. Methods Engrg. 55 (2002) 629–652.
[14] U. Andelfinger, E. Ramm, EAS-elements for two-dimensional, three-dimensional, plate and shell structures and their equivalence to HR-elements, Int. J. Numer. Methods Engrg. 36 (1993) 1311–1337.
[15] V.V. Novozhilov, The Theory of Thin Shells, P. Noordhoff, Ltd., Groningen, The Netherlands, 1959.
[16] A.L. Gol'denveizer, Theory of Elastic Thin Shells, Pergamon Press Ltd., Great Britain, 1961 (trans., orig. Russian vol.: Gostekhizdat, 1953).
[17] J. Pitkäranta, A.-M. Matache, C. Schwab, Fourier mode analysis of layers in shallow shell deformations, Comput. Methods Appl. Mech. Engrg. 190 (2001) 2943–2975.
[18] P. Karamian-Surville, J. Sanchez-Hubert, E. Sanchez-Palencia, Propagation of singularities and structure of layers in shells. hyperbolic case, Comput. Struct. 80 (2002) 747–768.
[19] E. Sanchez-Palencia, On internal and boundary layers with unbounded energy in thin shell theory. Elliptic case, Asymptot. Anal. 36 (2003) 169–185.
[20] L. Beirão da Veiga, Asymptotic energy behavior of two classical intermediate benchmark shell problems, Math. Models Methods Appl. Sci. (M^3AS) 13 (2003) 1279–1302.
[21] A.H. Niemi, J. Pitkäranta, H. Hakula, Benchmark computations on point-loaded shallow shells: Fourier vs. FEM, Comput. Methods Appl. Mech. Engrg. 196 (2007) 894–907.
[22] D. Caillerie, A. Raoult, E. Sanchez-Palencia, On internal and boundary layers with unbounded energy in thin shell theory. Hyperbolic characteristic and non-characteristic cases, Asymptot. Anal. 46 (2006) 189–220.
[23] D. Caillerie, A. Raoult, E. Sanchez-Palencia, On internal and boundary layers with unbounded energy in thin shell theory. Parabolic characteristic and non-characteristic cases, Asymptot. Anal. 46 (2006) 221–249.
[24] K. Gerdes, A.M. Matache, C. Schwab, Analysis of membrane locking in hp FEM for a cylindrical shell, Z. Angew. Math. Mech. 78 (1998) 663–686.
[25] J. Pitkäranta, Y. Leino, O. Ovaskainen, J. Piila, Shell deformation states and the finite element method: a benchmark study of cylindrical shells, Comput. Methods Appl. Mech. Engrg. 128 (1995) 81–121.
[26] R.H. MacNeal, A simple quadrilateral shell element, Comput. Struct. 8 (1978) 175–183.
[27] T.J.R. Hughes, T.E. Tezduyar, Finite elements based upon Mindlin plate theory with particular reference to the four-node bilinear isoparametric element, J. Appl. Mech. 48 (1981) 587–596.
[28] G. Wempner, D. Talaslidis, C.-M. Hwank, A simple and efficient approximation of shells via finite quadrilateral elements, J. Appl. Mech. 49 (1982) 115–120.
[29] K.-J. Bathe, E.N. Dvorkin, A four-node plate bending element based on Mindlin/Reissner plate theory and a mixed interpolation, Int. J. Numer. Methods Engrg. 21 (1985) 367–383.
[30] A.H. Niemi, J. Pitkäranta, Bilinear finite element for shells: isoparametric quadrilaterals, Int. J. Numer. Methods Engrg. (2007), doi:10.1002/nme.2252.
[31] J. Pitkäranta, The problem of membrane locking in finite element analysis of cylindrical shells, Numer. Math. 61 (1992) 523–542.
[32] J. Pitkäranta, M. Suri, Design principles and error analysis for reduced-shear plate-bending finite elements, Numer. Math. 75 (1996) 223–266.
[33] J. Pitkäranta, M. Suri, Upper and lower error bounds for plate-bending finite elements, Numer. Math. 84 (2000) 611–648.
[34] J. Pitkäranta, The first locking-free plane-elastic finite element: historia mathematica, Comput. Methods Appl. Mech. Engrg. 190 (2000) 1323–1366.
[35] D. Chapelle, K.-J. Bathe, The Finite Element Analysis of Shells: Fundamentals, Springer, Germany, 2003.
[36] V. Havu, J. Pitkäranta, Analysis of a bilinear finite element for shallow shells II: Consistency error, Math. Comput. 72 (2003) 1635–1653.
[37] V. Havu, J. Pitkäranta, Analysis of a bilinear finite element for shallow shells I: Approximation of inextensional deformations, Math. Comput. 71 (2002) 923–943.